Statistical characterization of arctic polar-night jet oscillation events

Statistical Characterization of Arctic Polar-Night Jet Oscillation Events

PETER HITCHCOCK AND THEODORE G. SHEPHERD

Department of Physics, University of Toronto, Toronto, Ontario, Canada

GLORIA L. MANNEY*

Jet Propulsion Laboratory, California Institute of Technology, Pasadena, California, and New Mexico Institute of Mining and Technology, Socorro, New Mexico

(Manuscript received 24 March 2012, in final form 9 August 2012)

ABSTRACT

A novel diagnostic tool is presented, based on polar-cap temperature anomalies, for visualizing daily variability of the Arctic stratospheric polar vortex over multiple decades. This visualization illustrates the ubiquity of extended-time-scale recoveries from stratospheric sudden warmings, termed here polar-night jet oscillation (PJO) events. These are characterized by an anomalously warm polar lower stratosphere that persists for several months. Following the initial warming, a cold anomaly forms in the middle stratosphere, as does an anomalously high stratopause, both of which descend while the lower-stratospheric anomaly persists. These events are characterized in four datasets: Microwave Limb Sounder (MLS) temperature observations; the 40-yr ECMWF Re-Analysis (ERA-40) and Modern Era Retrospective Analysis for Research and Applications (MERRA) reanalyses; and an ensemble of three 150-yr simulations from the Canadian Middle Atmosphere Model. The statistics of PJO events in the model are found to agree very closely with those of the observations and reanalyses.

The time scale for the recovery of the polar vortex following sudden warmings correlates strongly with the depth to which the warming initially descends. PJO events occur following roughly half of all major sudden warmings and are associated with an extended period of suppressed wave-activity fluxes entering the polar vortex. They follow vortex splits more frequently than they do vortex displacements. They are also related to weak vortex events as identified by the northern annular mode; in particular, those weak vortex events followed by a PJO event show a stronger tropospheric response. The long time scales, predominantly radiative dynamics, and tropospheric influence of PJO events suggest that they represent an important source of conditional skill in seasonal forecasting.

1. Introduction

The Arctic stratospheric polar vortex is one of the most variable features of the zonal-mean general circulation of the earth's atmosphere. This variability is driven by highly nonlinear interactions between the vortex and planetary-scale Rossby waves propagating upward from the troposphere. These dynamics manifest themselves most spectacularly in the form of stratospheric sudden warmings (SSWs) during which the climatological eastward flow reverses on time scales of a few days. In contrast to the suddenness of this onset, the vortex can in some cases take several months to recover to its climatological state. These extended recovery periods are the subject of this paper.

The methodology adopted here extends that of a body of work (Kodera et al. 1990, 2000; Kuroda and Kodera 2001, 2004), which identified the poleward and downward migrations of zonal-mean zonal wind anomalies on monthly time scales and termed them the polar-night jet oscillation (PJO). These slow migrations were first noted in the context of the 11-yr solar cycle (Kodera et al. 1990). The perspective taken by these studies is that the migrations constitute a mode of variability operating steadily throughout the winter with similar behavior for anomalies of both signs, albeit with

* Current affiliation: NorthWest Research Associates, and New Mexico Institute of Mining and Technology, Socorro, New Mexico.

Corresponding author address: Peter Hitchcock, Dept. of Applied Mathematics and Theoretical Physics, University of Cambridge, Wilberforce Road, Cambridge CB3 0WA, United Kingdom.
E-mail: aph42@cam.ac.uk

DOI: 10.1175/JCLI-D-12-00202.1

large variations in amplitude. That the far more rapid SSWs tend to occur in a particular phase of the PJO has been seen as a case of phase locking of the more rapid warmings onto the slower PJO (Kodera et al. 2000).

The claim made here is that the most coherent behavior captured by these statistical analyses is, in fact, more usefully considered as specific events: namely, the extended dynamical recovery of the vortex observed following some sudden warmings [except where noted explicitly, this paper will be concerned with major warmings (Charlton and Polvani 2007)]. Two particularly clear examples of such extended recoveries have been observed by the Microwave Limb Sounder (MLS) aboard the *Aura* satellite, following the warmings of 2006 and 2009. These recoveries are characterized by a vertical tripole structure in polar-cap-averaged temperature anomalies, with a persistently warm lower stratosphere, a cold middle to upper stratosphere, and a warm mesosphere. The latter corresponds to an unusually elevated stratopause (Siskind et al. 2007, 2010; Manney et al. 2008). While the anomaly in the lower stratosphere persists, the elevated stratopause descends over the course of several months. This pattern of evolution is shown here to be an extremely robust feature of the Arctic vortex, occurring following roughly half of all sudden warmings. To emphasize the connection with the slow migration described by the PJO and to stress that their behavior is distinct from that of sudden warmings in general, we term these as PJO events. In contrast to the linearity implied by the correlative analyses reviewed above, the phase progression of PJO events is always the same, in that the initial amplification of the polar anomaly is far more rapid than the subsequent downward migration, and coincides with a warming event. While the vortex at times does become anomalously cold and strong, such events do not possess the dynamic similarity shared by PJO events.

Numerous indices and events have been defined to characterize the variability of the Arctic vortex (e.g., Baldwin and Dunkerton 2001; Zhou et al. 2002; Kuroda and Kodera 2004; Charlton and Polvani 2007; Harnik 2009). We justify the introduction of a novel type of event, based on the PJO as defined by Kuroda and Kodera (2004), because we believe it to be a classification that

(i) is robust to small changes in the definition,
(ii) produces events that are similar to each other in some sense beyond the criteria used to define them,
(iii) affords novel understanding of the behavior of the vortex that is not accessible through existing definitions, and
(iv) captures similar events in a variety of datasets.

The PJO itself is defined by the principal component (PC) time series of the first two empirical orthogonal functions (EOFs) of polar-cap-averaged temperature profiles. To support the above claims, these are used to develop a novel tool for visualizing the daily variability of the Arctic vortex, in a fashion that is sufficiently compact that several decades of variability can be presented at once. This tool is applied to compare the detailed behavior of the Arctic vortex in MLS satellite observations, the 40-yr European Centre for Medium-Range Weather Forecasts Re-Analysis (ERA-40) and the National Aeronautics and Space Administration Modern Era Retrospective Analysis for Research and Application (MERRA), and the Canadian Middle Atmosphere Model (CMAM), a comprehensive chemistry climate model. The definition and statistical characterization of PJO events provides a means of testing several hypotheses regarding the origin of their long time scales.

These monthly time scales are likely closely related to the persistence of the lower-stratosphere circulation anomaly following the sudden warming. There are several reasons why such anomalies could exhibit such extended persistence. One simple idea is that the depth to which warming descends during a SSW is linked to its persistence (Gerber et al. 2009) via radiative time scales, which increase with decreasing altitude and are at their longest in the lower stratosphere (Dickinson 1973; Hitchcock et al. 2010). The depth of this descent has in turn been associated with the persistence of the waves that induced the warming (Zhou et al. 2002; Harnik 2009). Events triggered by a brief pulse of waves were found by Harnik (2009) to disrupt only the upper stratosphere, putting the vortex into a configuration favorable to reflect further waves, while those events triggered by an extended pulse disrupt the lower stratosphere as well. The descent of the warming plays a central role in the definition of PJO events introduced here, facilitating more detailed examination of these relationships.

The role of the radiative time scales in the extended persistence of the lower-stratospheric anomaly is, however, only one part of the dynamics. One must also understand why the eddies should remain quiescent over such extended periods. It has been shown in model studies that the radiative damping time scales do not necessarily have a strong impact on the persistence of the lower-stratospheric anomalies (Charlton-Perez and O'Neill 2010), suggesting this suppression is a nontrivial effect.

Both observational (Charlton and Polvani 2007) and modeling (Yoden et al. 1999) studies have suggested that warmings during which the polar vortex splits have longer time scales than those during which the vortex is displaced off the pole, indicating that the zonal wavenumber of the eddies may be significant. One rather

heuristic argument for why this should be is that the displacement of the vortex off the pole might in some sense be more dynamically reversible than the splitting of the vortex. Another possibility is suggested by work showing that vortex splits are more barotropic than vortex displacements (Matthewman et al. 2009) and are associated with a barotropic wave mode (Esler and Scott 2005; Liberato et al. 2007; Matthewman and Esler 2011), which would be expected to disrupt the lower-stratospheric vortex more efficiently than the vertically propagating modes responsible for vortex displacements. If the zonal-mean lower-stratospheric disturbance is of leading importance to the recovery time scale, the longer time scales associated with vortex splits could thus be more directly a consequence of the vertical structure of the wave driving, rather than the zonal wavenumber of the eddies.

Several studies have examined the elevated stratopause that occurs during PJO events (e.g., Siskind et al. 2007; Manney et al. 2008). The association of these events with extended time-scale sudden warmings noted by Siskind et al. (2010) is confirmed by the results presented here.

PJO events are also closely related to weak vortex events, as defined by Baldwin and Dunkerton (2001). The former dominate composites of the latter as a result of their large amplitudes, particularly at lags beyond two or three weeks. Previous studies have shown an equatorward shift of the tropospheric jets associated with both PJO (Kuroda and Kodera 2004; Kohma et al. 2010) and weak vortex events (Baldwin and Dunkerton 2001). Though the extended time scales of PJO events are suggested by the long decorrelation time scales (Baldwin et al. 2003; Gerber et al. 2010) of the northern annular mode (NAM), since these decorrelation time scales are a property of the whole time series their connection with specific events is not clear. The visualization tool and event definition introduced here is used to clarify these relationships, enhancing our understanding of polar vortex behavior [criterion (iii) above].

A similar comparison between the two leading EOFs of polar-cap-averaged temperatures was done on a 15 000-yr integration of a simplified general circulation model (Kohma et al. 2010). The classification of PJO events in the present work differs significantly in that the emphasis here is on the descent of the anomalies to the lower stratosphere. The variability of the vortex in the real atmosphere and in the comprehensive model is also expected to differ from the simplified model in which parameterized gravity waves were omitted.

The datasets used in this study are described in section 2. Section 3 introduces the novel visualization tool and the definition used to identify PJO events as well as reviews the two types of events that will be compared in detail with the PJO. In section 4 the robustness of the PJO definition is first tested explicitly in the reanalyses and the model, and then the relationship of sudden warmings and weak vortex events to PJO events is examined in detail. Conclusions are presented in section 5.

2. Data

Four datasets are analyzed in this paper: one set of satellite observations, two reanalysis products, and output from one chemistry climate model.

The MLS instrument on the *Aura* satellite has provided daily temperature profiles from the lowermost stratosphere through the mesosphere based on thermal microwave emissions from several chemical species (Schwartz et al. 2008). We make use of version 3.3 data (Livesey et al. 2011) from August 2004 through January 2011 and follow the recommended data quality screening procedures. The large vertical domain (from 316 to 0.001 hPa) and relatively good vertical resolution (on the order of 3 km in the stratosphere, degrading toward the lower stratosphere and upper mesosphere) provides a validation of the reanalysis data, which is of particular importance in the upper stratosphere and lower mesosphere where reanalyses show strong biases associated with the elevated stratopause (Manney et al. 2008).

To obtain a longer record of the observed vortex behavior, we turn to two reanalysis products. Data for 45 years from ERA-40 are used spanning from September 1957 through August 2002 (Uppala et al. 2005). The model underlying the data assimilation system has horizontal resolution T159 and 60 vertical levels from the surface to 0.1 hPa, though data are provided only up to 1 hPa. The quality of stratospheric temperatures, particularly prior to 1979, is limited to some degree by inhomogeneities in the assimilation of observations, as will be apparent. To include the most recent decade, data from MERRA spanning from January 1979 through April 2011 are also used (Rienecker et al. 2011). The resolution of the underlying model is 0.5° latitude by 0.75° longitude, finite volume, with 72 vertical levels up to 0.01 hPa. Data are available to 0.1 hPa. Combined, these products provide a record of 54 winters.

Model simulations permit even longer time series. CMAM is a chemistry climate model (CCM) that has participated in both recent phases of the SPARC Chemistry Climate Model Validation (CCMVal) activity (SPARC CCMVal 2010). We consider the ensemble of three ''REF2'' runs from the first CCMVal intercomparison; these are specified to include transient

forcing from projected emissions of greenhouse gases and ozone depleting substances. The runs span from 1950 to 2100; discarding the first decade for spinup, a total of 420 simulated years are available. Runs from the first phase of CCMVal are used because their Arctic circulation has been shown to compare very closely to reanalyses (McLandress and Shepherd 2009a; Hitchcock et al. 2009), both in its mean state and in its variability. This close agreement was unfortunately not obtained by the CMAM integrations submitted for the second CCMVal intercomparison (Butchart et al. 2011). The simulations were run at a horizontal resolution of T31 (5.6° × 5.6° linear transform grid) with 72 vertical levels from the surface to the upper mesosphere. They include comprehensive stratospheric chemistry (de Grandpré et al. 2000) and a full suite of physical parameterizations (Scinocca et al. 2008). Sea surface temperatures and sea ice concentrations in each ensemble member were specified from the output of three runs of a fully coupled tropospheric model forced by the same emissions scenarios.

3. Methods

The present goal is to characterize the variability of the vortex, not its sensitivity to secular changes. To control for the increase in frequency of sudden warmings identified in these runs by McLandress and Shepherd (2009a), we divide them into a present (1960–2010) and a future (2050–2100) period. The former is comparable to the period covered by the reanalyses considered here. However, note that, where quantities are found not to change appreciably over the course of the simulations, we include all simulated years in order to improve statistics.

Similarly, where quantities are established to not differ significantly between the two reanalyses or the greater vertical domain of MERRA is not of interest, the datasets are merged using ERA-40 data up to 31 December 1978 and MERRA data from 1 January 1979 onward, providing a single merged reanalysis record from September 1958 to April 2011.

To compute deseasonalized and detrended anomalies for the reanalyses and CMAM, we fit a linear trend at each grid point and day of the year. Then we smooth this background (mean and trend) by retaining only the first four harmonics of the annual cycle. This background is then subtracted from the field of interest to compute anomalies. This approach is similar to that outlined by Gerber et al. (2010): since the impact of ozone depletion on temperatures is considerably weaker in the Northern Hemisphere than in the Southern Hemisphere, we do not expect the use of a linear trend through the entire CMAM simulation period to significantly impact our results.

This procedure is modified slightly to compute temperature anomalies from the satellite data. Owing to the relatively short record, we omit the three winter seasons during the record with large PJO events: 2005/06, 2008/09, and 2009/10. The climatology is then computed from the remaining data, and no trend is removed. While this biases the climatology, it is preferable to the alternative since the large amplitude and similar timing of these events produces an artifact in the climatology that in turn affects the anomalies in other years. This issue is discussed further below.

a. Sudden warmings

Stratospheric sudden warmings are identified by reversals of the zonal-mean zonal wind at 10 hPa, 60°N using the criteria defined by Charlton and Polvani (2007). Note that there is a minor ambiguity in their prescription of how to remove reversals that occur in quick succession: here zonal wind reversals are considered warmings if they were not preceded by easterly winds at any time within the previous 20 days (Charlton-Perez and Polvani 2007, Corrigendum). In contrast, McLandress and Shepherd (2009a) used an interval of 60 days from the previous wind reversal identified as a warming. The former, when applied to the ERA-40, reproduces exactly the central dates in Table 2 of Charlton and Polvani (2007), and it is this criterion that is used in the present study.

The warmings are further divided into vortex splits and displacements through an independent implementation of the classification algorithm of Charlton and Polvani (2007), which is based on identifying vortex edges in the absolute vorticity at 10 hPa. A minor change is made here to their parameter n_c; 21 vorticity contours are constructed instead of 12. This was found to produce more reliable classifications in our implementation as compared to subjective inspection. The algorithm was applied to the model and the MERRA reanalysis; the subjective classification of Charlton and Polvani (2007) is used for ERA-40. The classification of SSWs in MERRA is summarized in Table 1 and agrees with the ERA-40 classifications to about the same degree as did the two reanalyses considered in Charlton and Polvani.

Since the occurrences of stratospheric sudden warmings (SSWs) in both reanalyses are in close agreement during their overlap period, we compare their combined statistics to those of the CMAM runs. Figures 1a, b compare the modeled to the observed occurrence of vortex splits and displacements as a function of month. Confidence intervals at the 95% significance level are estimated by assuming an event may happen each year

TABLE 1. SSW classification in MERRA: displacement (D) and split (S). The ERA-40 classification is that of Charlton and Polvani (2007) during the overlap period.

Central date		Type	
MERRA	ERA-40	MERRA	ERA-40
22 Feb 1979	22 Feb 1979	S	S
29 Feb 1980	29 Feb 1980	D	D
	4 Mar 1981		D
4 Dec 1981	4 Dec 1981	D	D
24 Feb 1984	24 Feb 1984	D	D
1 Jan 1985	1 Jan 1985	S	S
23 Jan 1987	23 Jan 1987	D	D
8 Dec 1987	7 Dec 1987	S	S
14 Mar 1988	14 Mar 1988	D	S
21 Feb 1989	21 Feb 1989	S	S
15 Dec 1998	15 Dec 1998	D	D
26 Feb 1999	26 Feb 1999	S	S
20 Mar 2000	20 Mar 2000	D	D
12 Feb 2001	11 Feb 2001	D	D
30 Dec 2001	30 Dec 2001	S	D
	17 Feb 2002		D
18 Jan 2003		D	
5 Jan 2004		D	
21 Jan 2006		D	
24 Feb 2007		D	
22 Feb 2008		D	
24 Jan 2009		S	
9 Feb 2010		S	
24 Mar 2010		D	

with probability p; this implies that the occurrence rate is drawn from a binomial distribution with n equal to the number of years. The parameter p is estimated from the occurrence rate of the type of event in question. Note that this neglects the possibility of multiple warmings in one year, as well as the possibility of serial correlations. The latter in particular would potentially increase the size of the error bars; these confidence intervals therefore represent a lower bound. The large intervals shown in Fig. 1 thus emphasize the difficulty of estimating these statistics even with over five decades of data. For instance, the deficit of modeled sudden warmings in January, common to many CCMs (Butchart et al. 2011) and attributable here to a deficit in vortex splits, lies within the confidence interval. Overall, the model produces vortex splits roughly half as often as have occurred in the real atmosphere (Fig. 1c), though again this difference lies within the confidence interval. The overall increase in the number of warmings in the model future (McLandress and Shepherd 2009a) is dominated by an increase in displacements.

b. Weak vortex events

The NAM indices are computed following Gerber et al. (2010). At each pressure level and each day, the global mean is removed from the zonal-mean geopotential height. This residual is then deseasonalized and detrended as discussed above. The first EOF is computed from area-weighted anomalies north of the equator, after Baldwin and Thompson (2009). We follow McLandress and Shepherd (2009a) and define strong and weak vortex events to occur when the PC time series rises above 1.5σ or falls below -2.5σ, respectively, and discard events that occur within 60 days of a prior event. These criteria were chosen by McLandress and Shepherd (2009a) so that the number of events identified in a reanalysis product matched the number of SSWs that occurred over the same period. A similarly close agreement is found here. The threshold for weak vortex events is slightly different from the -3σ threshold used by Baldwin and Dunkerton (2001): the sensitivity to this choice will be discussed below. Note that the 60-day interval here is from the previous date when the PC time series crossed the threshold; this is different from the 20-day interval required since the previous period of easterly winds in the SSW case.

c. Polar-night jet oscillation events

The PJO indices are defined following Kuroda and Kodera (2004) in terms of the first two EOFs of daily-mean polar-cap-averaged (70°–90°N) temperatures. Data from all seasons are included for continuity. The spatial structure of the EOFs is only weakly sensitive to these details. The first EOF describes a vertical dipole with one maximum near 1 hPa and the other near 0.01 hPa; the second EOF also describes a dipole, one-quarter wavelength out of phase with the first, with a lower maximum near 10 hPa (Fig. 2). We adopt the sign convention that a positive anomaly in the PC time series corresponds to a positive lower maximum—that is, to a warm upper stratosphere for EOF 1 and a warm middle stratosphere for EOF 2. The two EOFs together capture roughly 85% of the total daily variance, with a relatively large separation $\Delta\lambda \sim 20\%$ of the fraction of variance described by each EOF (see Table 2).

The two EOFs in the model and reanalyses agree to well within the 95% confidence intervals estimated by bootstrapping the model data into 7-yr subsamples (roughly the length of the MLS record). The EOFs from the satellite data show somewhat larger differences. In particular, the first EOF has a small negative feature in the lowermost stratosphere that is not present in either the model data or the reanalyses. However, if EOFs are computed from MERRA data from the same time period as the MLS observations the same lower-stratospheric structure is recovered (not shown), showing that this is a sampling issue. If we consider the total root-mean-square temperature amplitude of the two EOFs,

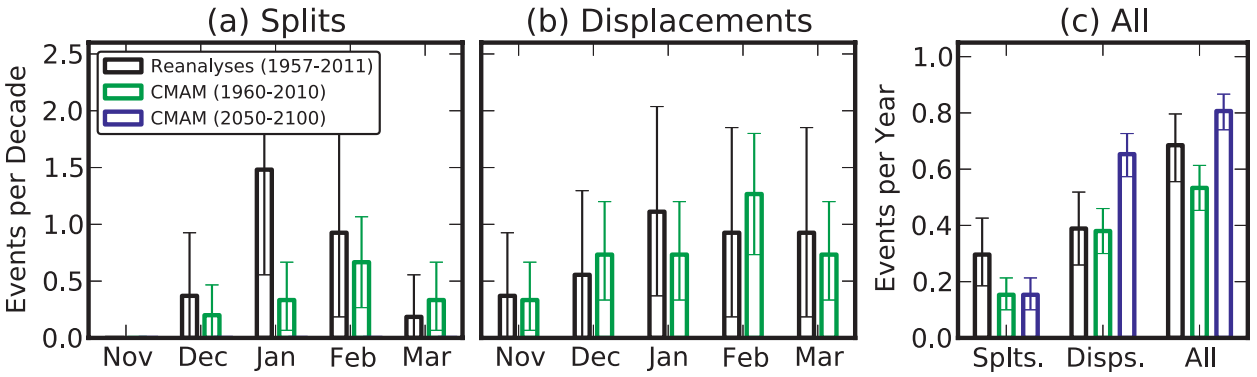

FIG. 1. Occurrence frequency of (a) splits and (b) displacements as a function of month for the reanalyses and CMAM datasets. (c) Net occurrence frequency for splits, displacements, and both combined. Statistics from the future period of the CMAM simulations are shown only in (c). Error bars indicate estimated 95% confidence intervals.

the MLS data agree well through the stratosphere, with only a small departure in the mesosphere. This suggests that the difference in the lower stratosphere is in the relative phase of the first two EOFs, which, despite the relatively good separation in their eigenvalues, is particularly susceptible to statistical uncertainty (North et al. 1982).

The PC time series (ts_1 and ts_2) corresponding to these two EOFs can be used to define a trajectory in a two-dimensional phase space (Kodera et al. 2000; Kuroda and Kodera 2004), which describes the evolution of the vertical structure of Arctic polar-cap-averaged temperature anomalies. We transform them to polar coordinates

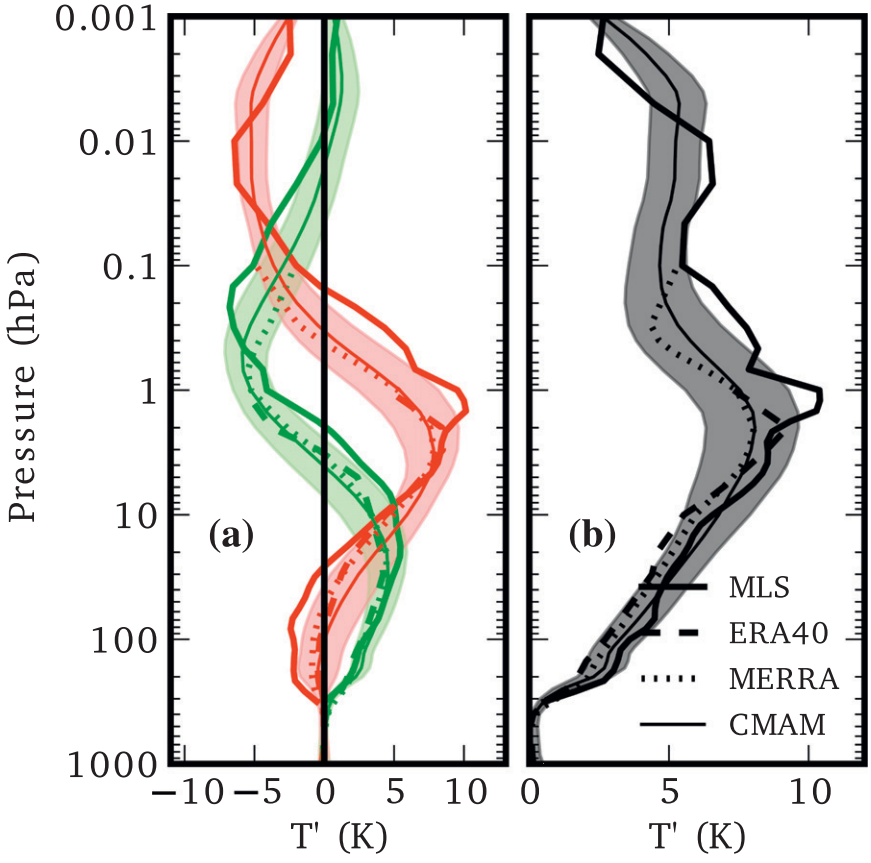

FIG. 2. (a) EOFs of polar-cap-averaged 70°–90°N temperatures; EOF 1 is shown in red and EOF 2 is shown in green as computed from the four datasets. (b) Rms amplitude of the first two EOFs. The shading indicates 2σ variability on 7-yr subsamples of the CMAM simulation (see text).

TABLE 2. Percentage of variance explained by the EOFs in Fig. 2. The uncertainties are estimated by bootstrapping the CMAM data.

	MLS	ERA-40	MERRA	CMAM
EOF 1	56% ± 6%	50% ± 3%	50% ± 3%	54%
EOF 2	32% ± 6%	27% ± 3%	35% ± 3%	31%

r and θ, defined by $r^2 = \mathrm{ts}_1^2 + \mathrm{ts}_2^2$ and $\tan\theta = \mathrm{ts}_2/\mathrm{ts}_1$. Examples of these are shown in Fig. 3. Figures 3a,b show MLS temperature anomalies during the winters 2007/08 and 2008/09 from November through April. The trajectories of the two winters in the phase space are shown in Figs. 3e,f. This approach has also been used in several other contexts (Wallace et al. 1993), though the irregularity of the PJO presents a significant challenge to the direct examination of these trajectories.

These trajectories are visualized more clearly and compactly by the colored "ribbons" in Figs. 3c,d. The width of the ribbon corresponds to the radial component r, or in more physical terms, to a vertically integrated, rms measure of the departure of the temperatures from climatological values. A reference width, corresponding to 2σ, is shown on the bottom left of each panel. The color corresponds to the phase of the trajectory θ or physically to the altitude of the local maximum in the profile of the temperature anomaly. The positive phase of EOF 1, in which the upper stratosphere is anomalously warm, is considered the positive x axis ($\theta = 0$) and is colored red. The positive phase of EOF 2, in which the middle stratosphere is anomalously warm, is considered the positive y axis ($\theta = \pi/2$) and is colored green. The negative phase of EOF 1 is colored blue, and the negative phase of EOF 2 is colored yellow. Phases intermediate to these four key directions are colored by interpolating linearly in red–green–blue (RGB) space. A legend is provided as an aid to the reader (Fig. 3g). For reasons that will shortly become apparent (see Fig. 4), we refer to these as "abacus" plots.

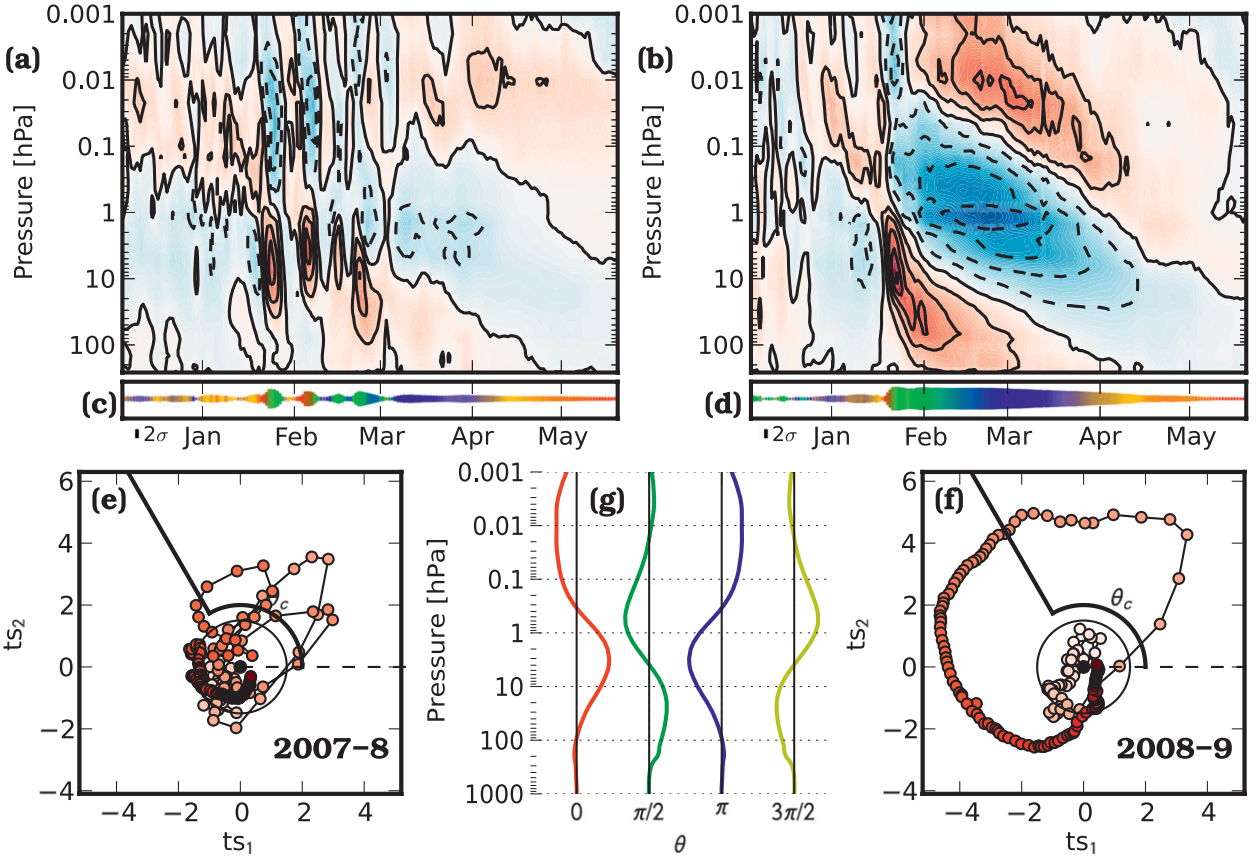

FIG. 3. Polar-cap temperature anomalies for the winters (a) 2007/08 and (b) 2008/09 from MLS: contour intervals 10 K. (c),(d) Corresponding abacus plots; see text for details. Ticks indicate the first of the month. (e),(f) Corresponding trajectories in the phase space defined by the first two EOFs. Symbols are marked each day over the winter season, shaded to indicate the date: white for days early in the season, darkening to red for days late in the season. (g) Legend for abacus plot coloring. Vertical structure of temperature anomalies as a function of θ.

The winter of 2007/08 featured four brief episodes of upper-stratospheric warming and lower-mesospheric cooling between late January and the end of February (Fig. 3a). Only the last warming (during which the winds at 10 hPa reverse) reaches the lower stratosphere. These episodes are well described by the first two EOFs, though they are difficult to identify in the phase-space trajectory. The corresponding abacus plot, however, shows four episodes during which the ribbon broadens, allowing their timing and relative amplitudes to be easily compared. The blue color in the final episode indicates the lower-stratospheric warming. The ability to show both amplitude and vertical structure of the polar warming at daily resolutions is the main advantage of the abacus plots.

The major sudden warming of 2008/09 exhibits clearly the evolution of temperature anomalies characteristic of PJO events as described in the introduction (Fig. 3b). This is captured by the EOFs as a rapid initial amplification, followed by a slow rotation in the EOF phase space (Fig. 3f). It shows up in the abacus plot as a rapid broadening of the ribbon and coincident change in color from red to green, followed by a slow change of color from green to blue to yellow as the anomalies descend (Fig. 3g). By the end of the descent the trajectory has performed nearly one complete rotation.

That PJO events similar to this are ubiquitous and evident in abacus plots will be seen shortly. It is, however, useful to be able to identify these events algorithmically. A PJO event is defined here to occur when the trajectory rotates through a specific phase θ_c, provided the amplitude is greater than a threshold r_c. At this point the vertical profile of temperature anomalies has a local maximum at a particular pressure corresponding to the value of θ_c. This criterion is illustrated in Figs. 3e,f; an event is identified when the trajectory crosses the bold ray counterclockwise. This is referred to as the central date, though it need not occur at the midpoint between the start and end dates defined below. To define the duration of the event, we consider it to begin on the first date prior to the central date when the amplitude exceeds another threshold r_m (where $r_m < r_c$) and to end on the first date following the central date when the amplitude falls again below r_m. This lower threshold is shown in Figs. 3e,f by the thin inner circle. To reduce the impact of small fluctuations of the trajectory near these threshold points, ts_1 and ts_2 are smoothed by a 5-day low-pass filter prior to applying the above definition. This smoothing is not performed in any other analyses done here.

Unless otherwise noted, a standard reference phase of $\theta_c = 2\pi/3$ is used. In all cases, threshold amplitudes of $r_c = 2\sigma$ and $r_m = 1.5\sigma$ are used. Sensitivity to the definition of these parameters is discussed further below. Note that this definition is intended to select events based on a particular height to which the maximum in the vertical profile of the temperature anomalies descends. For the standard reference phase, this local maximum lies at 60 hPa.

Finally, to correct for the slight phase differences between the various datasets associated with the EOF analysis, ts_1 and ts_2 for the two reanalyses are computed by projecting their temperature anomalies onto the CMAM EOFs. This results in only minor changes to ts_1 and ts_2 but, since the compositing technique depends on their relative phase, the projection facilitates the comparison between the reanalyses and the model, in accordance with criterion (iv) proposed in the introduction.

4. Results

Abacus plots for all years of the three observational/reanalysis datasets and for one century (1980–2080) of one member of the CMAM ensemble are shown in Fig. 4. Polar-night jet oscillation (PJO) events, identified as described above, are indicated on the abacus plots by the vertical black lines. The dates of sudden warmings are also indicated by horizontal lines, and weak vortex events are indicated by downward-opening chevrons. Further annotations are described below.

The ubiquity of the long, slow evolution of the PJO is apparent in all datasets in the characteristic red-to-green-to-blue tails. Although about 85% of PJO events in the reanalyses are initiated by a sudden warming, more than 50% of sudden warmings are not followed by a PJO event, even in midwinter (e.g., December 2001 and January 2003). They are similarly associated with weak vortex events. We take the similarity between PJO events and their association with only a subset of sudden warmings and weak vortex events as evidence that the present definition satisfies criterion (ii) proposed in the introduction. There are nonetheless a few periods identified as PJO events during which a sudden warming does not occur. In some cases (e.g., January 1998) the episode is identified as a weak vortex event though the formal criteria for a sudden warming are never met. (Indeed, the correspondence between sudden warmings and weak vortex events is perhaps weaker than one might expect, though a more thorough consideration of this question is beyond the scope of this work.) Other cases are indicative of minor limitations in the algorithmical procedure for defining PJO events; for instance, the events identified in November 1996 and November 2009 in MERRA differ qualitatively from the more typical midwinter events. These false positives are not frequent enough to be of concern to the

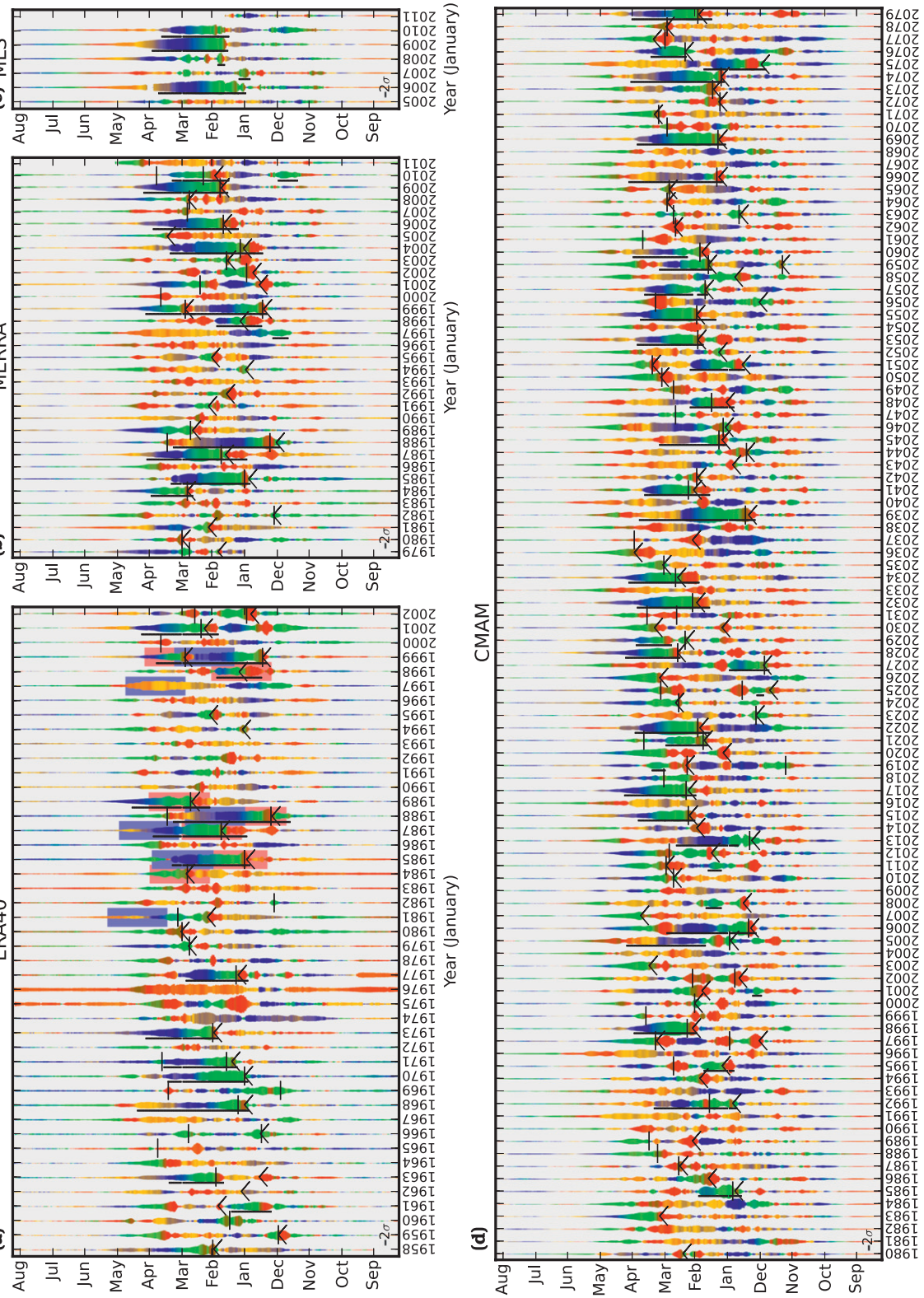

FIG. 4. Abacus plots for (a) ERA-40, (b) MERRA, (c) MLS, and (d) 100 years from one member of the CMAM ensemble. Sudden warmings are indicated by horizontal lines; weak vortex events are indicated by downward-opening chevrons. PJO events are indicated by a vertical line to the left of the abacus ribbon. See text for further details.

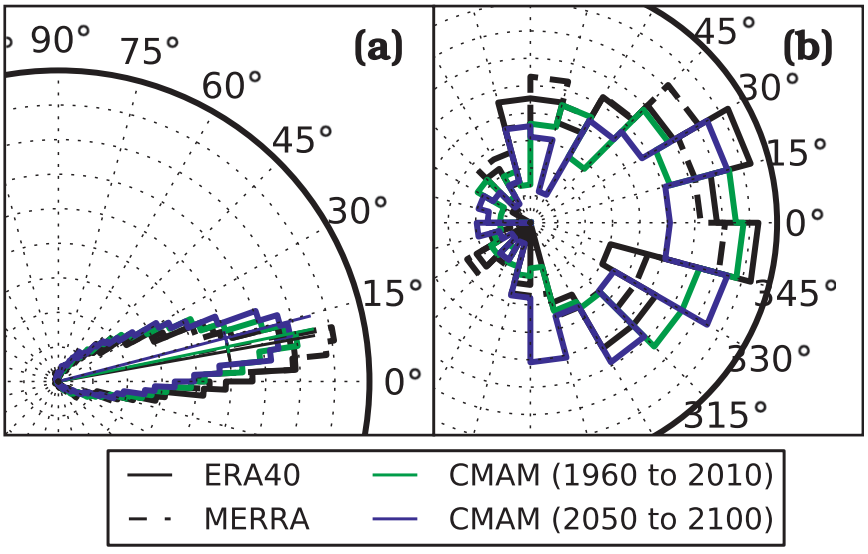

FIG. 5. Histogram of (a) the change in θ over 5 days for initial states with $r > 1.5\sigma$ and (b) the phase when r increases by more than 2.5σ in 5 days.

conclusions; the parameters of the definition were chosen to strike a reasonable balance between their occurrence and the occurrence of false negatives such as the recovery in MERRA from the vortex split of March 1989.

The qualitative agreement between the reanalyses and the satellite observations during the overlap periods is for the most part very good (cf. from 1979 to 2002 of ERA-40 and MERRA; from 2005 to 2011 of MERRA and MLS). The phase shift between the CMAM and MLS EOFs is apparent in the abacus plot in that PJO events in the model and reanalyses begin with a longer red phase (consider the three large PJO events in 2006, 2009, and 2010). In all datasets the initial warming begins in the upper stratosphere and does not involve a cooling of the lower stratosphere; that this behavior is described by different linear combinations of the MLS EOFs than of the CMAM EOFs accounts for the apparent difference in the character of the initial red phase of the PJO events in the two datasets. The two short events identified in January 2007 and 2008 are also due to this phase difference.

There are some small quantitative differences between the reanalyses. For instance, the sudden warming in February 2001 is classified as a PJO event in ERA-40, but the temperature anomalies it induces are not quite large enough to be classified as such in MERRA. There is an artifact during 1975–76 in the ERA-40 dataset that projects onto EOF 1; this results in the wide red band that persists through the year. This is likely associated with a known error in the bias-correction of data from the National Oceanic and Atmospheric Administration *NOAA-4* satellite, which affects upper-stratospheric temperatures during this period (Uppala et al. 2005). The reanalysis prior to 1979, apart from this anomaly, looks qualitatively similar to that in the satellite-era data.

The qualitative character of the variability in the model vortex also agrees quite well with the reanalyses. The long red-to-green-to-blue tails characteristic of PJO events are similarly ubiquitous (Fig. 4d), confirming that their definition satisfies proposed criterion (iv).

As an example of the utility of abacus plots for comparing indices of variability in the Arctic stratosphere, the episodes of descending warm and cold anomalies studied by Zhou et al. (2002) are also indicated on the ERA-40 abacus plot as wide red and blue ribbons, respectively. The descending warm anomalies can be seen to correspond to the early phase of PJO events. The cold anomalies that tend to follow the descending warm anomalies correspond to a later phase of PJO events (with the exception of the events beginning in March 1981 and March 1997).

As a coarse characterization of ts_1 and ts_2, Fig. 5 shows histograms of two quantities. Figure 5a shows histograms of the rotation rate in the reanalyses and model (computed here as the change in phase over five days for all dates with amplitudes greater than 1.5σ), showing the typical counterclockwise rotation of the EOFs (or physically the downward propagation of temperature anomalies). The mean rates agree well between all three datasets (ERA-40: 2.0° ± 0.6° day^{-1}, MERRA: 2.3° ± 0.9° day^{-1}, and CMAM to present: 2.3° ± 0.4° day^{-1}). Taking the wavelength of the EOFs to be roughly 50 km, these correspond to a mean propagation of about −300 m day^{-1}, significantly faster than typical polar residual vertical velocities ($\overline{w}^* \approx -50$ m day^{-1}). The

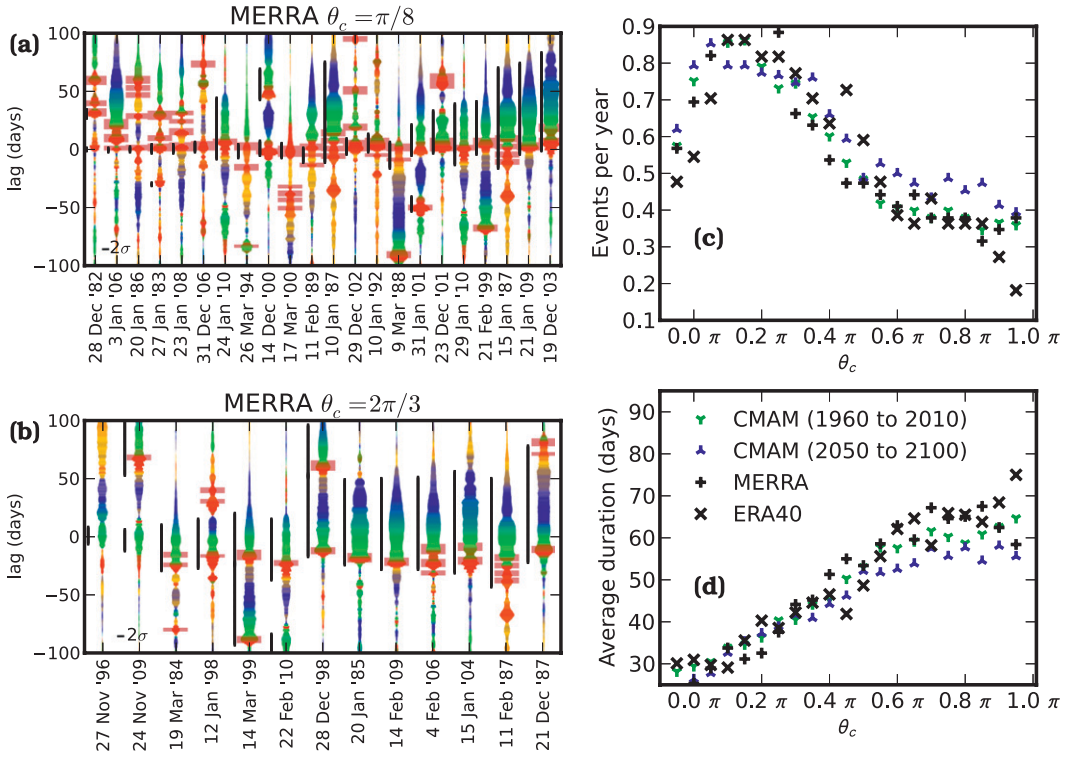

FIG. 6. Sensitivity of event definition to the reference phase θ_c. (a),(b) Events from MERRA with reference phase $\theta_c = \pi/8$ and $2\pi/3$. Vertical lines indicate PJO events as classified by the corresponding value of θ_c. Wide dark red ribbons indicate periods when the reflective index (see text) is greater than 2σ. (c) The number of events identified per year vs θ_c for both reanalysis datasets and the past and future periods of the CMAM simulations. (d) The mean duration in days of events identified vs θ_c for the same datasets.

rotation rate in the model accelerates with climate change, to $2.9° \pm 0.4°$ day^{-1} over the last five decades of the run. Although the relationship between the rotation rate and $\overline{w}^*$ is not straightforward, this change may be associated with the acceleration of the Brewer–Dobson circulation (McLandress and Shepherd 2009b).

Figure 5b shows the distribution of phases during rapid amplifications of the temperature anomalies (defined here as a change in $r > 2.5\sigma$ over 5 days). The reanalyses and the model show a peak in this distribution near $\theta = 0$, indicating that amplifications tend to occur during the positive phase of EOF 1. Physically, this indicates that the largest and most rapid warming typically occurs in the upper stratosphere. Consistent with the easterly pseudomomentum carried by Rossby waves and with prior composite studies (e.g., Limpasuvan et al. 2005), warm events tend to develop more rapidly and to larger amplitudes than cold events.

The event definition itself provides a means of testing the relationship between the depth of the warming and its time scale. Figure 6 shows the sensitivity of the event definition to the choice of the reference phase θ_c. Figures 6a,b show events from MERRA for two choices, $\theta_c = \pi/8$ and $2\pi/3$, respectively. They are then sorted by the amplitude of the event at the central date.

The central date for the events identified in Fig. 6a corresponds to an anomalously warm upper stratosphere: the temperature anomaly at this phase peaks at 5 hPa. Most of these events are minor warmings confined to the upper stratosphere (the pulse remains red), and the temperature anomaly amplifies and then decays within at most a few weeks. Only a few PJO events are also captured, suggesting that the upper-stratospheric warming during PJO events is not as strong as during the minor warmings identified here. This is consistent with the separate peaks in the distribution of warming events found by Kohma et al. (2010) in a mechanistic model. Also shown in these plots is the reflective index (the difference between the zonal-mean zonal wind averaged from 53° to 74°N at 10 and 2 hPa) introduced by Perlwitz and Harnik (2004). Following Harnik (2009), periods when the index falls below -13.4 m s^{-1} (two standard deviations) are indicated on the abacus plots. These correspond closely to the reflective events identified by Harnik (2009).

The events identified in Fig. 6b, in contrast, have much longer time scales. The phase progression (red to green

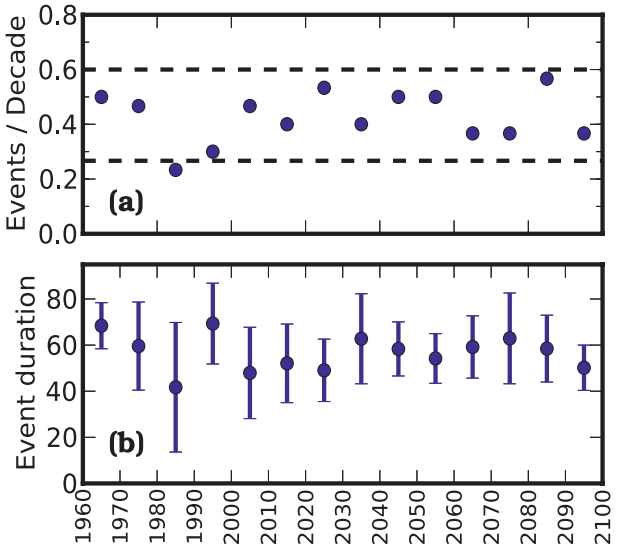

FIG. 7. (a) PJO event frequency in events per year from the CMAM ensemble. The dashed lines indicate the expected 95% confidence interval for a 30-yr sample assuming a constant occurrence rate (see text). (b) PJO event duration in days for each decade, with 95% confidence intervals.

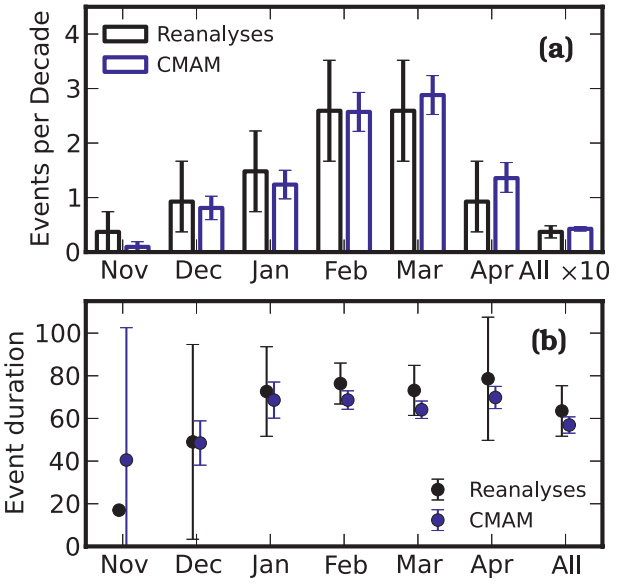

FIG. 8. (a) PJO event occurrence frequency in events per decade for merged reanalyses and CMAM ensemble, as a function of month and in events per year for all events (rightmost column). (b) Average PJO event duration in days as a function of month and for all events.

to blue to yellow) corresponding to the downward-propagating temperature anomalies is also more apparent. As noted by Harnik (2009), during these events the vortex initially goes into a strongly reflective configuration. In these cases, however, wave activity continues to be absorbed by the mean flow and the warming descends to the lower stratosphere (recall that $\theta_c = 2\pi/3$ corresponds to a peak warming near 60 hPa). These events also occur less frequently than minor warmings: only 13 events are identified compared to the 22 identified in Fig. 6a. In part this is due to their long time scales; no more than two such events occur in a season and two (e.g., 1998–99) is an unusual occurrence.

Figures 6c,d demonstrate the robustness of these relationships. Figure 6c shows the number of events identified per year as a function of θ_c for the reanalyses and the present and future periods of the CMAM simulations. The frequency of events peaks near the $\pi/8$ case shown in Fig. 6a and falls off steadily as θ_c increases. The number of events also falls off for $\theta_c < \pi/8$. This dependence is reproduced by both reanalyses and the model simulations. Figure 6d shows the average duration of the events. The time scales lengthen steadily with the depth of the warming, as suggested by Gerber et al. (2009).

Sensitivity of the definition to the parameters r_c and r_m has also been explored, though these are of less physical interest. The reanalyses are nearly completely insensitive to r_c for values between 1.6 and 2.4 σ, though this may be a result of inadequate sampling as the number and duration of events identified in CMAM is weakly sensitive in this range. Over a broader range the sensitivities of the three datasets are roughly the same, with fewer and longer events being identified as r_c increases. Varying the value of r_m does not affect the number of events identified, though their duration decreases as r_m increases. Note that, in the case of the two PJO events identified in 1998–99, the amplitude of the PJO drops to less than 1.5σ, so they are identified as nonoverlapping events by the standard choice of r_m.

There is a weak suggestion in Fig. 6c of an increase in the number of PJO events projected by CMAM. That this is not in fact the case is demonstrated in Fig. 7a, which shows the ensemble-averaged frequency by decade. To test the significance of any trend, we take as a null hypothesis that the occurrence rate is fixed at p events per year over the 140 years of the simulation. As with the SSW occurrence rate, we estimate the 95% confidence interval on a 30-yr sample drawn from a binomial distribution; this interval is indicated by the dashed lines in Fig. 7a. One of the 14 decades in the simulation lies slightly below the confidence interval, which is to be expected for the given level of significance. There is, therefore, no statistical evidence of a trend in the number of PJO events occurring in these simulations. This is consistent with the results of McLandress and Shepherd (2009a) given that, like the NAM-based events for which they found no trend and unlike sudden

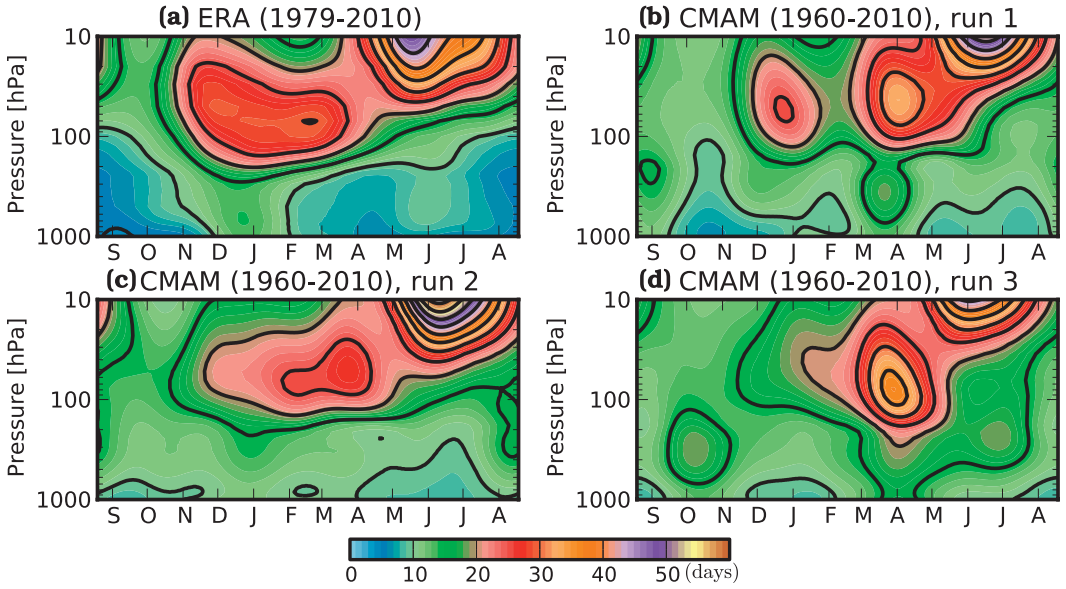

FIG. 9. Northern annular mode decorrelation time scales for (a) ERA-Interim for the period 1979–2010 and (b)–(d) each of the three members of the CMAM ensemble for the period 1960–2010: contours at intervals of 5 days.

warmings for which they did, the PJO indices are computed after removing a slowly varying background trend.

Similarly, there is no evidence for a trend in the mean duration of the PJO events in these simulations (Fig. 7b). On the basis of these results, we can then make use of the entire simulation period of the ensemble to consider, in Fig. 8, the seasonal dependence of PJO statistics. Figure 8a shows the frequency of events by month for the model and the merged reanalyses (considering each separately reveals no significant differences). Error bars are estimated as described above. Since events typically span several months, an event is considered to have occurred in a given month if any date between its onset and its conclusion falls within that month. A significant number of events persist through April. These are not necessarily final warmings since the warming that initiates them often occurs in February (e.g., the warmings in February 1989, February 2001, or even January 1968).

Figure 8b shows the average duration of events that occur in each month. The seasonal cycle of event duration is relatively weak, with early winter (November and December) events persisting for somewhat shorter periods than the rest of the extended winter period. This weak seasonal cycle is to some extent an artifact of how we include events in each month; a similar plot showing the duration of only those events whose central dates lie in a given month shows that those events that are identified in February and March do tend to be somewhat shorter than those identified in January, likely because their amplitude attenuates rapidly once the summer season begins, leaving less time for events that begin later in the season to persist (not shown).

The agreement in all cases between model and reanalyses is well within the estimated sampling error. PJO events in the reanalyses occur at a rate of 3.7 ± 1.1 events per decade, while those in the model simulations occur at a rate of 4.3 ± 0.4 events per decade. The close agreement between both duration and frequency of PJO events in the model and the reanalyses raises the question of how closely these time scales correspond to the decorrelation times of the annular mode. Chemistry climate models are known to exhibit long biases in these decorrelation time scales (Gerber et al. 2010), though the statistical significance of this bias in the Northern Hemisphere has recently been questioned (Simpson et al. 2011).

To check this hypothesis, the decorrelation time scales of the northern annular mode are shown in Fig. 9 as a function of pressure and season. They are computed following the method of Simpson et al. (2011). The time scales in the lower stratosphere computed from the ERA-Interim for 1979–2010 (Fig. 9a) peak during December–February (DJF) near 30 days. Time scales for each of the three CMAM ensemble members for 1960–2010 (Figs. 9b–d) during DJF vary from 15 to 25 days, though there is considerable variability despite the use of 50 years of data. There is a peak in April in two of the runs, which resembles the multimodel ensemble mean shown in Gerber et al. (2010). At any rate, the apparent biases in these decorrelation times do not correspond with the close agreement in PJO duration seen in Fig. 8,

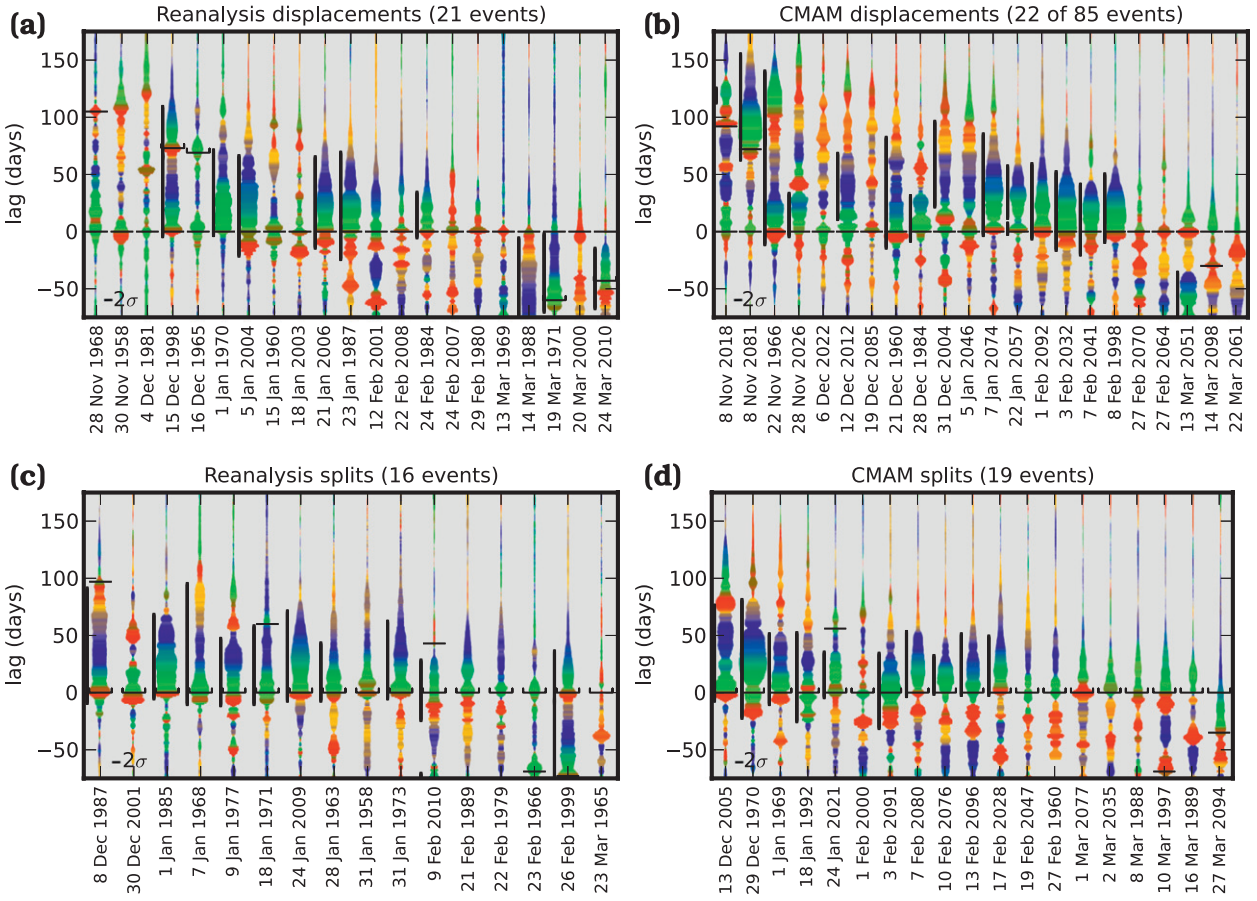

FIG. 10. Abacus plots of SSW events, divided into (top) vortex displacements and (bottom) vortex splits; the events are sorted by when they occur in the season. Lag zero is taken as the central date of the sudden warming. PJO events are indicated as in Fig. 4. Sudden warmings are indicated by horizontal lines, with upticks added to vortex splits in this figure only to distinguish them from vortex displacements. Events (left) from the merged reanalysis data and (right) from one ensemble member of the CMAM model runs. For CMAM, every fourth displacement is selected (prior to sorting) for clarity.

which suggests that these long events are not the sole determinant of the decorrelation time scales.

a. Relationship to sudden warmings

Nearly every PJO event as identified here follows a stratospheric sudden warming. However, the reverse is not true: many sudden warmings are not followed by PJO events.

Making use of the sudden warming classifications described above, we now divide the sudden warming events in the merged reanalyses and in the model into splits and displacements. Figure 10 shows abacus plots for every observed sudden warming (displacements in top panels and splits in the bottom). Of the 21 observed vortex displacement events, 6 are followed by a PJO event as identified by the event definition, while a seventh (in February 2001) is followed by an extended recovery, though not of large enough amplitude to meet the PJO criterion. In contrast, 10 of the 16 observed vortex splits are classified as PJO events, while 2 or 3 more (January 1958, February 1989, and possibly February 1979) have extended time scales with weaker amplitudes. Notably, the February 1979 warming, which has been studied extensively as an archetypical vortex split (e.g., Matthewman et al. 2009, and references therein), had a fairly weak impact on the vortex temperatures. This is also consistent with the measure of the temperature change reported by Charlton and Polvani (2007).

The odds of these warmings being followed by a PJO event are summarized in Table 3. Although there is a suggestion that observed vortex splits are more frequently followed by PJO events than are vortex displacements, the short observational record precludes a definitive conclusion. Indeed, two examples of strong PJO events following clear vortex displacement events have occurred in the past decade (in January 2004 and

TABLE 3. PJO occurrence following sudden warmings.

Event type	Fraction followed by PJO events		Duration of PJO events (days)	
	CMAM	Reanalyses	CMAM	Reanalyses
All	0.40 ± 0.06	0.43 ± 0.16	65 ± 4	72 ± 10
Split	0.56 ± 0.12	0.6 ± 0.3	62 ± 7	71 ± 15
Displacement	0.36 ± 0.06	0.3 ± 0.2	66 ± 5	75 ± 20

January 2006). Assuming the observed probabilities, at least 100 years of observations would be required to distinguish these at the 95% significance level. Note that the durations of PJO events following splits and displacements are indistinguishable.

As noted above (Fig. 1c), vortex splits in CMAM occur roughly half as often as in the observations, though this difference is not statistically significant. The fraction of splits and displacements followed by PJO events nonetheless agrees well with the reanalyses; furthermore, the long integrations provide sufficient statistics to differentiate the two, supporting the suggestion that PJO events do occur more frequently following vortex splits. As in the observations, the duration of PJO events following each type of warming is indistinguishable. The results of Table 3 indicate that the suggestion of Charlton and Polvani (2007) that vortex splits take longer to recover than do vortex displacements arises because of the greater tendency for the former to be followed by a PJO event.

As has been noted in previous studies (Limpasuvan et al. 2004; Charlton and Polvani 2007; Liberato et al. 2007), the flux of planetary wave activity entering the vortex following sudden warmings is reduced. We note here that this suppression is much more striking during PJO events than during non-PJO events. Figure 11 shows composites of the (absolute) zonal-mean zonal wind, area averaged from 50° to 70°N, and the anomalous vertical component of the Eliassen–Palm (EP) flux, area averaged from 50° to 90°N. The former is representative of the peak zonally averaged winds of the vortex, while the latter range includes the bulk of the upward flux of wave activity entering the polar vortex. The results are not strongly sensitive to either latitude range. Regions where the EP flux does not differ significantly from the climatology at the 95% confidence level are hatched. The left panels of Fig. 11 show sudden warming events (both splits and displacements) that are not followed by a PJO event; the two reanalysis products have been divided here because of their different vertical domains and the potential for sponge-layer issues. On average, the zero-wind line descends just below the 10-hPa level required to meet the WMO criterion; moreover, the 10 m s^{-1} contour does not descend much lower than the 100-hPa level and, by 15 days following the central date, winds throughout the stratosphere are greater than 10 m s^{-1}. The pulse of EP flux responsible for the deceleration of the winds is apparent; following the wind reversal, however, the fluxes are only reduced significantly for perhaps 10 days.

Composite averages of warmings followed by a PJO event (Fig. 11, right) show somewhat more persistent easterly winds in the middle stratosphere (15 days compared to 5 days), but on average the zero-wind line does not differ drastically from the composite average of the non-PJO events. The 10 m s^{-1} contour, however, descends to the upper troposphere, and these weak westerlies persist for 40 days. The initial pulse of wave activity is again apparent and, as noted by Harnik (2009), is of considerably longer duration than during short-time-scale events. In contrast to the short-time-scale events, the vertical EP fluxes into the polar vortex are strongly suppressed for some 60 days following the initial wind reversal. This reduction is substantially less pronounced in the non-PJO composite, though it does remain significant for nearly as long as in the PJO composite. This significance may also be a consequence of false negatives in the algorithm used to defined PJO events: at short lags the composite will be dominated by the behavior of the more numerous shorter-time-scale events, while at long lags these will (on average) exhibit climatological behavior leaving the longer time-scale events to dominate the composite. The superrecovery of the upper-stratospheric jet during PJO events, consistent with the strong cold anomalies in the middle to upper stratosphere (as in Fig. 3b), is also apparent.

It is likely that the coherent, robust pattern of circulation anomalies exhibited during PJO events (apparent in Fig. 4) is a consequence of the strongly suppressed upward EP flux. In the absence of intermittent wave driving, the far more linear radiative processes will dominate the dynamics. Note that a simple application of the Charney–Drazin criterion requiring westerly winds for upward propagation (Charney and Drazin 1961) does not suffice to explain the suppressed waves, given the presence of westerly winds throughout the stratosphere. Moreover, filtering of waves by the stratospheric flow does not immediately explain the anomaly in the upward fluxes in CMAM, which extends down to the surface. Note that tropospheric fluxes in the reanalyses are too noisy to confirm this behavior in the real atmosphere. The suppression of upward fluxes in the troposphere of CMAM could in principle be explained by reflection (i.e., a cancellation between the upward and downward fluxes); note, however, that the reflective index of Perlwitz and Harnik (2004), which depends on the vertical shear between 10 and 2 hPa, suggests that

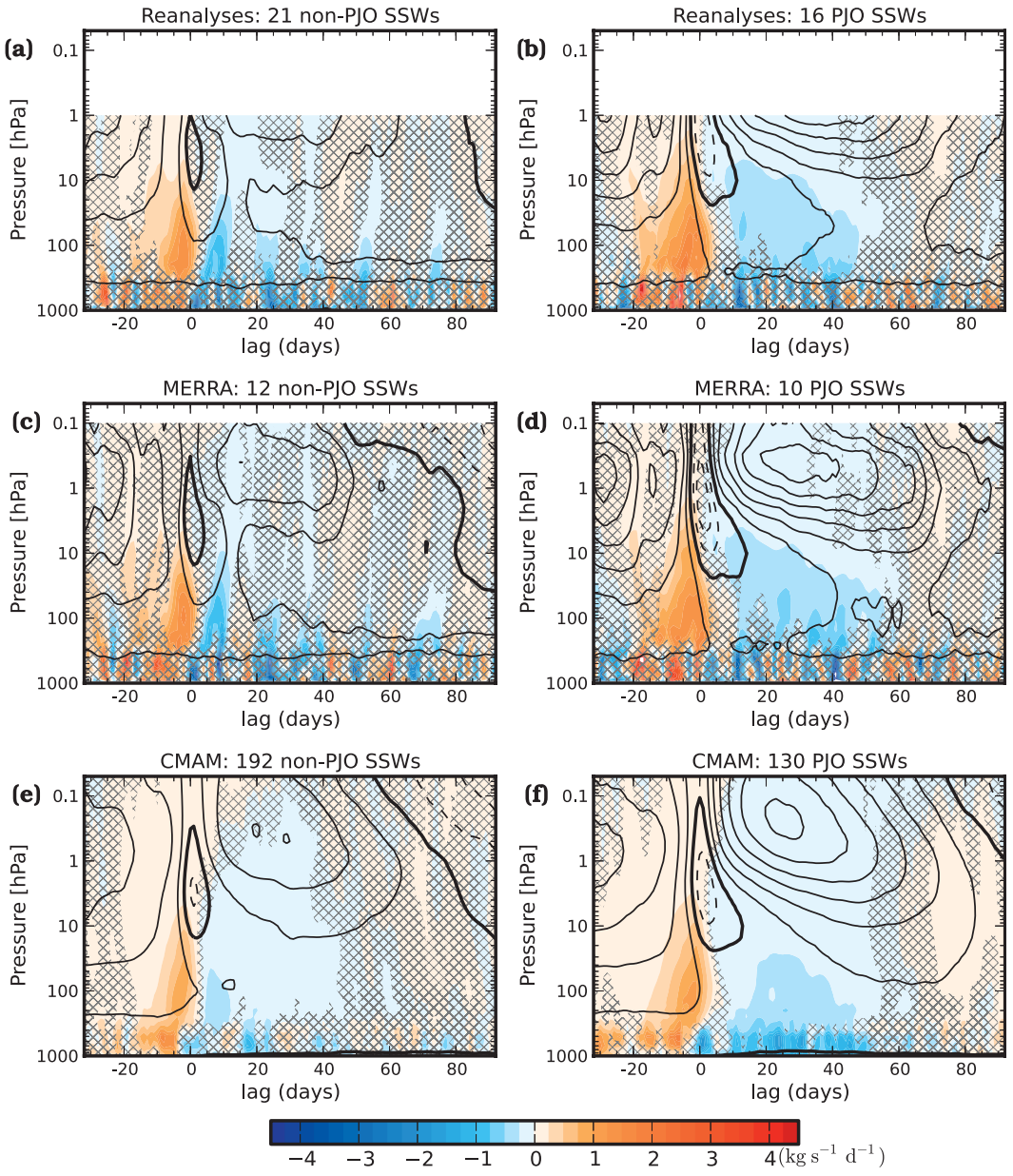

FIG. 11. Composites of zonal-mean zonal wind from 50° to 70°N (contours at 10 m s^{-1} intervals; zero contour is thick) and vertical EP flux anomalies from 50° to 90°N (color shading; kg s^{-1} day^{-1}). Regions in which the EP fluxes do not differ significantly from climatology at the 95% confidence level are hatched. Composite events are drawn from (a),(b) merged reanalyses; (c),(d) MERRA; and (e),(f) CMAM; the lag is measured from the central date of the SSW. Sudden warming events that are not followed by a PJO event are shown in (a),(c),(e); those events that are followed by a PJO event are shown in (b),(d),(f).

the vortex is in an extremely unfavorable configuration for reflection during this period.

b. *Relationship to weak vortex events*

PJO events are also closely related to the weak vortex events shown by Baldwin and Dunkerton (2001) to have a significant impact on the tropospheric annular mode. Abacus plots of the weak vortex events in the merged reanalysis dataset and in one ensemble member of the model are shown in Fig. 12. With a definition threshold of -2.5σ, somewhat less than half (15 of 40) of the weak vortex events in the merged reanalysis dataset are also classified as PJO events. The events in the abacus plots are sorted by the minimum value reached by the annular mode index over the 10 days following the -2.5σ threshold central date; increasing this threshold would

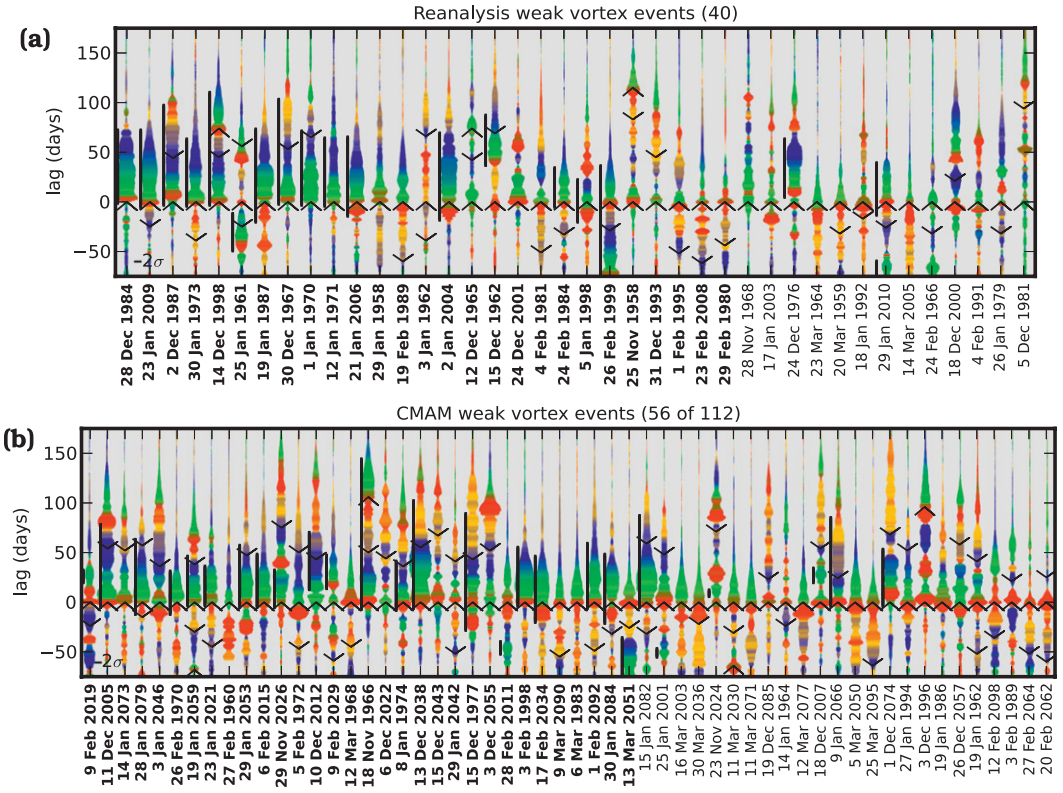

FIG. 12. Abacus plots of weak vortex events in the merged reanalyses and of every second event in one ensemble member of the CMAM simulations. Lag zero is taken as the central date of the weak vortex event. PJO events are indicated as in Fig. 4. Weak vortex events are indicated by downward opening chevrons, and strong vortex events are indicated by upward opening chevrons. The events are sorted by the minimum reached by the 10-hPa NAM index within 10 days of the event date; those that reach below -3σ are indicated by the bold labels.

therefore remove events from the right-hand side of the plot. Those events that would still be classified by a -3σ threshold are identified by the bold labels; this suggests that PJO events are more likely to occur following larger amplitude events. This is quantified in Table 4; PJO events follow roughly 40% of -2.5σ events, rising somewhat to 50% following -3σ events.

Strong vortex events are also indicated in Fig. 12 by upward-opening chevrons. During many of the largest PJO events, the superrecovery of the vortex seen in Fig. 11 is in fact strong enough to meet the 1.5σ threshold. The recovered vortex at this phase of the PJO events is unusually high as well as strong (the low polar temperatures imply large vertical shears by thermal wind balance), so these events tend to have a much stronger signature in the middle to upper stratospheric NAM indices than they do in the lower stratosphere. This differs qualitatively from other strong events visible in Fig. 12 that do not occur during PJO events (e.g., consider those preceding the weak vortex events in February 1995, February 1981, and January 1979). This lack of similarity between strong vortex events suggests that posing a definition for them that satisfies criterion (ii) would be problematic.

A similar picture emerges from the corresponding model abacus plot. Half of the weak vortex events from one ensemble member are shown in Fig. 12b as a representative sample. The fraction of weak vortex events followed by PJO events in the model agrees well with reanalyses for both the -2.5σ and -3σ threshold definitions (Table 4). The broad range of qualitative behaviors of strong vortex events is also apparent in the model.

If the equatorward shift of the tropospheric jets following weak vortex events is in fact caused by the lower-stratospheric anomalies (as suggested by Baldwin and Dunkerton 2001), then those events that have more

TABLE 4. Probability of PJO occurrence following weak vortex events.

NAM threshold	CMAM	Reanalyses
-2.5σ	0.41 ± 0.06	0.38 ± 0.15
-3σ	0.52 ± 0.07	0.5 ± 0.18

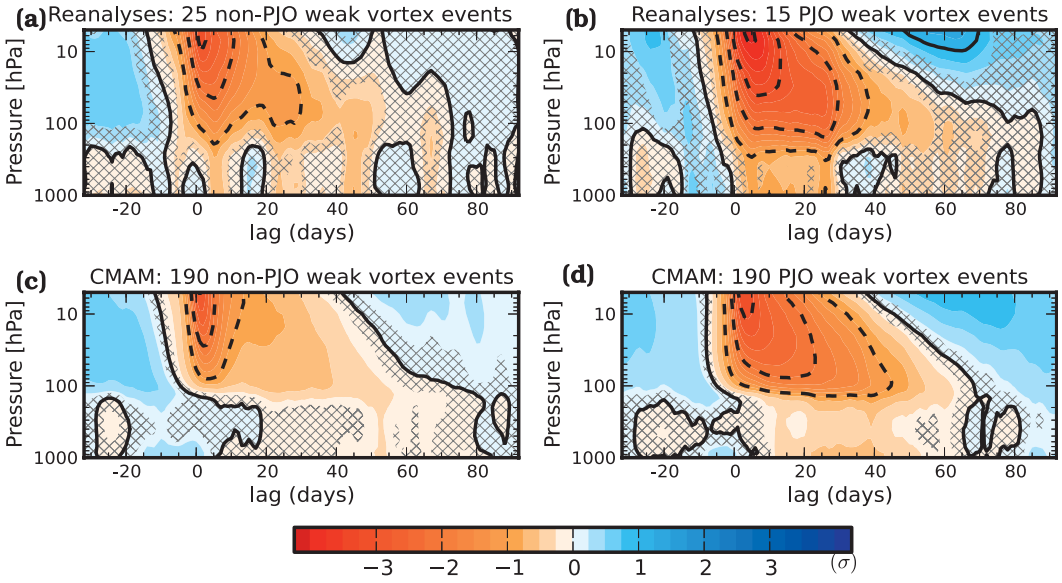

FIG. 13. As in Fig. 11 but for composites of the northern annular mode following weak vortex events. Events are drawn from (a),(b) the merged reanalyses and (c),(d) CMAM, for (a),(c) weak vortex events not followed by PJO events and (b),(d) weak vortex events followed by PJO events. The lag is measured from the central date of the weak vortex event. Shading and intervals indicate the NAM index: contour intervals at 1σ. Significance is indicated as in Fig. 11.

persistent such anomalies ought to have a greater impact on the troposphere. The impact of the PJO on the tropospheric circulation has been noted before (Kuroda and Kodera 2004; Kohma et al. 2010); the close correspondence between weak vortex events and PJO events, however, makes it difficult to determine if additional information is gained in the PJO perspective. Simplified model studies have indicated that longer time-scale variability in the stratosphere does correlate with stronger stratosphere–troposphere coupling (Gerber and Polvani 2009).

We therefore divide the weak vortex events into those events that correspond to PJO events and those that do not. Composites are presented in Fig. 13. The different character of non-PJO and PJO events in the reanalysis composites is shown in Figs. 13a,b. The stratospheric NAM anomaly in the latter is larger, and a -2σ anomaly persists for nearly 30 days. In contrast, the -2σ anomaly during non-PJO events on average persists for only 10 days. The tropospheric impact of PJO events is stronger and more coherent than that of non-PJO events, but even in the merged dataset the number of events is still too small to resolve differences in the tropospheric impact unambiguously.

Here the benefits of the long CMAM simulations are clear. Corresponding composites for non-PJO events (Fig. 13c) and PJO events (Fig. 13d) confirm the difference in the stratospheric signature of the two sets of events; PJO events have a much stronger, deeper, and longer anomaly above the tropopause. Their tropospheric impact is also considerably stronger: after roughly a 10-day lag from the onset of the stratospheric anomaly, the tropospheric annular mode follows suit, and negative anomalies remain while the lower-stratospheric anomaly persists. As with the reanalysis composite, a weak but statistically significant stratospheric anomaly persists for nearly as long during the non-PJO events, despite the much shorter central feature. While the tropospheric impact is negligible for the first 40 days following the non-PJO events, a weak but significant response arises from days 40–80. As with the reduced upward EP fluxes, this may be a consequence of false negatives. The tropospheric impact of PJO events is at any rate significantly stronger than that of non-PJO events.

5. Conclusions

A novel classification has been proposed to describe the extended, dynamical recovery of the Arctic polar vortex observed following a subset of major sudden warmings. A key tool, the ‘‘abacus’’ plot, used to demonstrate the value of this classification has also been introduced. This tool permits the compact visualization of up to several decades of Arctic polar vortex variability on daily time scales, based on the vertical structure of polar-cap-averaged temperature anomalies. In particular, this visualization makes clear that roughly one-half of stratospheric sudden warmings are followed by an

extended recovery phase characterized by a persistent lower-stratospheric warm anomaly, a cold anomaly that forms in the middle to upper stratosphere and descends, and an elevated stratopause that descends as well. We have referred to these episodes as PJO events, to emphasize both that they exhibit the most coherent manifestation of the poleward and downward migration of zonal wind and temperature anomalies termed the polar-night jet oscillation by Kuroda and Kodera (2001) and that they are dynamically distinct from the more general category of sudden warmings. These events are well captured by MLS satellite observations and the ERA-40 and MERRA reanalyses and are well simulated by the ensemble of CCM simulations considered here.

The objective definition of these events applied here is based on the PC time series of the same EOFs used to construct the abacus plots and distinguishes events based on the depth to which the initial warming descends. The definition meets the four criteria set out in the introduction: it is robust to small changes in the parameters of the definition, captures a set of events that share a number of key physical features, and describes similar events in a number of datasets.

Moreover, the statistical characterization of these events has provided a number of novel insights and helped to clarify and make more explicit some results suggested by previous studies. The duration of warming events is strongly correlated with the depth to which the initial warming descends, suggesting that the long time scales are closely related to the radiative damping time scales in the lowermost stratosphere. Just as essential for the long time scale of PJO events, however, is the strong suppression of upward fluxes of wave activity for the duration of the events. These fluxes are suppressed for much longer during PJO events than they are following non-PJO sudden warmings. Indeed, this distinction between PJO and non-PJO sudden warmings is highly relevant for the dynamics of the recovery of the vortex, suggesting that it is reasonable to consider this a key feature of PJO events. While this suppression is likely related to the disruption of the lower-stratospheric vortex, a simple application of the Charney–Drazin criterion is not sufficient to explain it since lower-stratospheric westerlies recover long before the waves do.

PJO events occur following both vortex displacement and vortex split sudden warmings, but do so somewhat more frequently following the latter. However, the splitting of the vortex is not a necessary condition. Moreover, the duration of PJO events is not sensitive to whether the initial sudden warming is a split or a displacement, which suggests, as was hypothesized in the introduction, that the zonally asymmetric component of the dynamics is important to the time scale of the recovery only insofar as it determines in part the vertical structure of the initial wave driving.

Finally, PJO events are also strongly associated with weak vortex events as identified by the NAM index at 10 hPa. They occur somewhat more frequently following weak vortex events of larger magnitude. The larger and more persistent lower-stratospheric anomalies associated with PJO events are associated with a stronger and more persistent tropospheric annular mode response.

The abacus plots are, more generally, particularly useful for comparing indices of Arctic polar vortex variability. For instance, they make evident the fact that PJO events correspond closely to the descending warm events identified by Zhou et al. (2002) and to the persistent wave driving events identified by Harnik (2009). Both of these studies suggested that an extended period of wave driving is required to disturb the lower stratosphere, a result confirmed by the composites of PJO sudden warmings.

As a dominant feature of the variability of the Arctic polar vortex, PJO events are highly likely to play a role in the response to many external perturbations, most notably the 11-yr solar cycle (Kodera et al. 1990; Ineson et al. 2011). Some properties of their behavior are also likely to be of considerable interest to seasonal forecasts in the northern extratropics. In particular, the behavior of planetary-scale eddies is likely the most challenging component of the Arctic circulation to forecast, given the highly relaxational (and hence predictable) nature of the radiative cooling. The suppression of wave activity during PJO events suggests, therefore, that stratospheric predictability may be enhanced during this period. The enhanced tropospheric response seen following PJO events further suggests that this predictability may lead to enhanced seasonal forecasts in the northern extratropics. These events may therefore represent a significant potential source of conditional skill at seasonal time scales. If so, a key question regarding the utility of abacus plots for identifying these events in real time is whether the definition of PJO events proposed here is optimal for identifying the conditions required for the planetary wave suppression.

Acknowledgments. We are grateful to Shigeo Yoden for many helpful discussions, particularly during an extended visit by PH under the Japan Society for the Promotion of Science summer program. We thank William Daffer for providing the polar-cap temperature data from MLS, Michael Neish and Isla Simpson for technical assistance accessing the CMAM model data, and two anonymous reviewers for their helpful comments. We also acknowledge the support of the Natural Sciences and Engineering Research Council and the

Canadian Foundation for Climate and Atmospheric Sciences. Work at the California Institute of Technology Jet Propulsion Laboratory was done under contract with the National Aeronautics and Space Administration.

REFERENCES

Baldwin, M. P., and T. J. Dunkerton, 2001: Stratospheric harbingers of anomalous weather regimes. *Science,* **294,** 581–584, doi:10.1126/science.1063315.

——, and D. W. J. Thompson, 2009: A critical comparison of stratosphere–troposphere coupling indices. *Quart. J. Roy. Meteor. Soc.,* **135,** 1661–1672, doi:10.1002/qj.479.

——, D. B. Stephenson, D. W. J. Thompson, T. J. Dunkerton, A. J. Charlton, and A. O'Neill, 2003: Stratospheric memory and skill of extended-range weather forecasts. *Science,* **301,** 636–640, doi:10.1126/science.1087143.

Butchart, N., and Coauthors, 2011: Multimodel climate and variability of the stratosphere. *J. Geophys. Res.,* **116,** D05102, doi:10.1029/2010JD014995.

Charlton, A. J., and L. M. Polvani, 2007: A new look at stratospheric sudden warmings. Part I: Climatology and modeling benchmarks. *J. Climate,* **20,** 449–469; Corrigendum, **24,** 5951.

Charlton-Perez, A. J., and A. O'Neill, 2010: On the sensitivity of annular mode dynamics to stratospheric radiative time scales. *J. Climate,* **23,** 476–484.

Charney, J. G., and P. G. Drazin, 1961: Propagation of planetary-scale disturbances from the lower into the upper atmosphere. *J. Geophys. Res.,* **66,** 83–109.

de Grandpré, J., S. R. Beagley, V. I. Fomichev, E. Griffioen, J. C. McConnell, A. S. Medvedev, and T. G. Shepherd, 2000: Ozone climatology using interactive chemistry: Results from the Canadian Middle Atmosphere Model. *J. Geophys. Res.,* **105** (D21), 26 475–26 491.

Dickinson, R. E., 1973: Method of parameterization for infrared cooling between altitudes of 30 and 70 kilometers. *J. Geophys. Res.,* **78,** 4451–4457.

Esler, J. G., and R. K. Scott, 2005: Excitation of transient Rossby waves on the stratospheric polar vortex and the barotropic sudden warming. *J. Atmos. Sci.,* **62,** 3661–3682.

Gerber, E. P., and L. M. Polvani, 2009: Stratosphere–troposphere coupling in a relatively simple AGCM: The importance of stratospheric variability. *J. Climate,* **22,** 1920–1933.

——, C. Orbe, and L. M. Polvani, 2009: Stratospheric influence on the tropospheric circulation revealed by idealized ensemble forecasts. *Geophys. Res. Lett.,* **36,** L24801, doi:10.1029/2009GL040913.

——, and Coauthors, 2010: Stratosphere-troposphere coupling and annular mode variability in chemistry-climate models. *J. Geophys. Res.,* **115,** D00M06, doi:10.1029/2009JD013770.

Harnik, N., 2009: Observed stratospheric downward reflection and its relation to upward pulses of wave activity. *J. Geophys. Res.,* **114,** D08120, doi:10.1029/2008JD010493.

Hitchcock, P., T. G. Shepherd, and C. McLandress, 2009: Past and future conditions for polar stratospheric cloud formation simulated by the Canadian Middle Atmosphere Model. *Atmos. Chem. Phys.,* **9,** 483–495, doi:10.5194/acp-9-483-2009.

——, ——, and S. Yoden, 2010: On the approximation of local and linear radiative damping in the middle atmosphere. *J. Atmos. Sci.,* **67,** 2070–2085.

Ineson, S., A. A. Scaife, J. R. Knight, J. C. Manners, N. J. Dunstone, L. J. Gray, and J. D. Haigh, 2011: Solar forcing of winter climate variability in the Northern Hemisphere. *Nat. Geosci.,* **4,** 753–757, doi:10.1038/ngeo1282.

Kodera, K., K. Yamazaki, M. Chiba, and K. Shibata, 1990: Downward propagation of upper stratospheric mean zonal wind perturbation to the troposphere. *Geophys. Res. Lett.,* **17,** 1263–1266.

——, Y. Kuroda, and S. Pawson, 2000: Stratospheric sudden warmings and slowly propagating zonal-mean zonal wind anomalies. *J. Geophys. Res.,* **105** (D10), 12 351–12 359.

Kohma, M., S. Nishizawa, and S. Yoden, 2010: Classification of polar-night jet oscillations and their relationship to fast and slow variations in a global mechanistic circulation model of the stratosphere and troposphere. *J. Climate,* **23,** 6438–6444.

Kuroda, Y., and K. Kodera, 2001: Variability of the polar night jet in the Northern and Southern Hemispheres. *J. Geophys. Res.,* **106** (D18), 20 703–20 713.

——, and ——, 2004: Role of the Polar-night Jet Oscillation on the formation of the Arctic Oscillation in the Northern Hemisphere in winter. *J. Geophys. Res.,* **109,** D11112, doi:10.1029/2003JD004123.

Liberato, M. L. R., J. M. Castanheira, L. de la Torre, C. C. DaCamara, and L. Gimeno, 2007: Wave energy associated with the variability of the stratospheric polar vortex. *J. Atmos. Sci.,* **64,** 2683–2694.

Limpasuvan, V., D. W. J. Thompson, and D. L. Hartmann, 2004: The life cycle of the Northern Hemisphere sudden stratospheric warmings. *J. Climate,* **17,** 2584–2596.

——, D. L. Hartmann, D. W. J. Thompson, K. Jeev, and Y. L. Yung, 2005: Stratosphere-troposphere evolution during polar vortex intensification. *J. Geophys. Res.,* **110,** D24101, doi:10.1029/2005JD006302.

Livesey, N. J., and Coauthors, 2011: Version 3.3 level 2 data quality and description document. Jet Propulsion Laboratory Tech. Rep. JPL D-33509, 162 pp. [Available online at http://mls.jpl.nasa.gov/data/v3-3_data_quality_document.pdf.]

Manney, G. L., and Coauthors, 2008: The evolution of the stratopause during the 2006 major warming: Satellite data and assimilated meteorological analyses. *J. Geophys. Res.,* **113,** D11115, doi:10.1029/2007JD009097.

Matthewman, N. J., and J. G. Esler, 2011: Stratospheric sudden warmings as self-tuning resonances. Part I: Vortex splitting events. *J. Atmos. Sci.,* **68,** 2481–2504.

——, ——, A. J. Charlton-Perez, and L. M. Polvani, 2009: A new look at stratospheric sudden warmings. Part III: Polar vortex evolution and vertical structure. *J. Climate,* **22,** 1566–1585.

McLandress, C., and T. G. Shepherd, 2009a: Impact of climate change on stratospheric sudden warmings as simulated by the Canadian Middle Atmosphere Model. *J. Climate,* **22,** 5449–5463.

——, and ——, 2009b: Simulated anthropogenic changes in the Brewer–Dobson circulation, including its extension to high latitudes. *J. Climate,* **22,** 1516–1540.

North, G. R., T. L. Bell, R. F. Cahalan, and F. J. Moeng, 1982: Sampling errors in the estimation of empirical orthogonal functions. *Mon. Wea. Rev.,* **110,** 699–706.

Perlwitz, J., and N. Harnik, 2004: Downward coupling between the stratosphere and troposphere: The relative roles of wave and zonal mean processes. *J. Climate,* **17,** 4902–4909.

Rienecker, M. M., and Coauthors, 2011: MERRA: NASA's modern-era retrospective analysis for research and applications. *J. Climate,* **24,** 3624–3648.

Schwartz, M. J., and Coauthors, 2008: Validation of the Aura Microwave Limb Sounder temperature and geopotential height measurements. *J. Geophys. Res.,* **113,** D15S11, doi:10.1029/2007JD008783.

Scinocca, J. F., N. A. McFarlane, M. Lazare, J. Li, and D. Plummer, 2008: The CCCma third generation AGCM and its extension into the middle atmosphere. *Atmos. Chem. Phys.,* **8,** 7055–7074.

Simpson, I. R., P. Hitchcock, T. G. Shepherd, and J. F. Scinocca, 2011: Stratospheric variability and tropospheric annular-mode timescales. *Geophys. Res. Lett.,* **38,** L20806, doi:10.1029/2011GL049304.

Siskind, D. E., S. D. Eckermann, L. Coy, J. P. McCormack, and C. E. Randall, 2007: On recent interannual variability of the Arctic winter mesosphere: Implications for tracer descent. *Geophys. Res. Lett.,* **34,** L09806, doi:10.1029/2007GL029293.

——, ——, J. P. McCormack, L. Coy, K. W. Hoppel, and N. L. Baker, 2010: Case studies of the mesospheric response to recent minor, major, and extended stratospheric warmings. *J. Geophys. Res.,* **115,** D00N03, doi:10.1029/2010JD014114.

SPARC CCMVal, 2010: SPARC report on the evaluation of chemistry-climate models. SPARC Rep. 5, WCRP Rep. 132, and WMO Tech. Doc. 1526, 434 pp.

Uppala, S. M., and Coauthors, 2005: The ERA-40 Re-Analysis. *Quart. J. Roy. Meteor. Soc.,* **131,** 2961–3012.

Wallace, J. M., R. L. Panetta, and J. Estberg, 1993: Representation of the equatorial stratospheric quasi-biennial oscillation in EOF phase space. *J. Atmos. Sci.,* **50,** 1751–1762.

Yoden, S., T. Yamaga, S. Pawson, and U. Langematz, 1999: A composite analysis of the stratospheric sudden warmings simulated in a perpetual January integration of the Berlin TSM GCM. *J. Meteor. Soc. Japan,* **77,** 431–445.

Zhou, S., A. J. Miller, J. Wang, and J. K. Angell, 2002: Downward-propagating temperature anomalies in the preconditioned polar stratosphere. *J. Climate,* **15,** 781–792.